Article

Iterative design of polymer fabric cathode for metal-ion batteries

Jun Guo [a,b,1], Hongbo Chen [c,1], Dapeng Wang [c], Wanqiang Liu [a,*], Gang Huang [b,*], Xinbo Zhang [b,*]

[a] School of Materials Science and Engineering, Changchun University of Science and Technology, Changchun 130022, China
[b] State Key Laboratory of Rare Earth Resource Utilization, Changchun Institute of Applied Chemistry, Chinese Academy of Sciences, Changchun 130022, China
[c] State Key Laboratory of Polymer Physics and Chemistry, Changchun Institute of Applied Chemistry, Chinese Academy of Sciences, Changchun 130022, China

A R T I C L E I N F O

A B S T R A C T

Organic electrode materials (OEMs) have attracted significant attention for use in aqueous zinc-ion batteries (AZIBs) because of their abundant resources and flexible designability. However, the development of high-performance OEMs is strongly hindered by their high solubility, poor conductivity, sluggish ion diffusion kinetics, and difficult coordination toward Zn^{2+}. Herein, inspired by fabric crafts, we have designed a robust polymer fabric through the iterative evolution of the building blocks from point to line and plane. The evolution from point to line could not only improve the structural stability and electrical conductivity but also adjust the active site arrangement to enable the storage of Zn^{2+}. In addition to further boosting the aforementioned properties, the evolution from line to plane could also facilitate the construction of noninterference channels for ion migration. Accordingly, the poly(1,4,5,8-naphthalenetetracarboxylic dianhydride/2,3,5,6-tetraaminocyclohexa-2,5-diene-1,4-dione) (PNT) polymer fabric has the most enhanced structural stability, optimized active site arrangement, improved electrical conductivity, and suitable ion channels, resulting in a record-high capacity retention of 96% at a high mass loading of 56.9 mg cm^{-2} and a stable cycle life of more than 20,000 cycles at 150 C (1 C=200 mA g^{-1}) in AZIBs. In addition, PNT exhibits universality for a wide range of ions in organic electrolyte systems, such as Li/Na/K-ion batteries. Our iterative design of polymer fabric cathode has laid the foundation for the development of advanced OEMs to promote the performance of metal-ion batteries.

1. Introduction

The generation of high-performance rechargeable batteries is vital to relieve the energy crisis and regulate the conflicts between humans and nature arising from the rapid development of technology [1]. In the past three decades, a substantial volume of research has been focused on the study of inorganic cathode materials, such as metallic oxides [2]. Nevertheless, the performance of this type of cathode materials has reached their theoretical values, limiting the further improvement of the performance of batteries, not to mention their resource-constrained nature [3]. In addition, inorganic materials, in general, follow an intercalation/conversion mechanism during the ion storage/release process, usually accompanied by large volume and crystal lattice changes, triggering the pulverization of inorganic materials and consequently leading to rapid capacity decay and short cycle life. By contrast, organic electrode materials (OEMs) with soft lattices stand out because of their unique coordination reaction toward ions, environmental friendliness, cost-effectiveness, and resource sustainability [4]. The unique ion storage mechanism of OEMs enables them to accommodate ions with different valences and sizes, especially the polyvalent Zn^{2+}, which can be used to construct high-performance aqueous zinc-ion batteries (AZIBs) that can cater to the needs of large-scale energy storage systems [5]. However, the storage process of Zn^{2+} in OEMs requires the synergy of multiple adjacent active sites and the occurrence of redox reactions in both surface and bulk phases to liberate their full performance potential [6]. Therefore, the active site arrangement and ion diffusion capability of OEMs are of great importance for their energy storage process. The high solubility and poor conductivity of OEMs also impose limitations on their application potential [7–10]. Although traditional polymerization or carbon recombination strategies could play certain roles, they cannot address the aforementioned issues at the same time and will usually have some negative effects, such as the reduction of energy density by the introduction of inactive

components [11,12]. More importantly, to the best of our knowledge, there is currently no work considering the construction of ion diffusion channels within the OEMs, which is particularly crucial for the fabrication of truly practical batteries that require electrodes with high mass loading. The diffusion of ions in the bulk electrode materials is the rate-limiting step for the electrode process and is thus important for the overall reaction kinetics of batteries. In this case, delving into the intricate interplay between the structure of OEMs and their corresponding stability, active site arrangement, electrical conductivity, and ion diffusion capability would provide a promising path to fully realize the benefits of OEMs and, accordingly, boost the performance of batteries.

With this in mind, we have designed a molecular construction process that starts from point to line and plane through the elaborate combination of building blocks, aiming to elucidate the impact of structural conformation of OEMs on electrochemical performance. The structural evolution from point to line could benefit molecular stability, electrical conductivity, and active site arrangement. Meanwhile, the structural evolution from line to plane with the building of polymer fabric not only leads to further enhancement of the aforementioned properties but also, more significantly, constructs unobstructed channels for ion migration, consequently unleashing the full performance potential of OEMs. This structural design process for OEMs not only represents the first exploration of its kind but also simultaneously addresses the fundamental challenges inherent in the existing classes of OEMs. As a result, the poly(1,4,5,8-naphthalenetetracarboxylic dianhydride/2,3,5,6-tetra aminocyclohexa-2,5-diene-1,4-dione) (PNT) polymer fabric exhibits exceptional cycling stability (i.e., 71% capacity retention over 2900 h at 0.5 C (1 C=200 mA g^{-1}) and 8% capacity fade after 20,000 cycles at 150 C) and surprising mass loading insensitivity (i.e., above 96% capacity retention even with the increase in mass loading to 56.9 mg cm^{-2}). Furthermore, the inherent stability and unobstructed ion migration channels of PNT also make it suitable for storing Li^+/Na^+/K^+ in organic electrolyte systems with high reversible capacities, superior rate capability, and long-term stability.

2. Experimental

The details of the material synthesis, characterizations, electrochemical measurements, and theoretical calculations are provided in the Supplementary materials (online).

3. Results and discussion

3.1. Structural evolution of OEMs from point to line and plane

Dianhydride-based molecules have the potential to be high-performance OEMs because of their large theoretical capacities [13]. However, their intrinsic broadband gaps and densely packed structure, similar to that of the basic dianhydride-based molecule (1,2,3,4-cyclobutanetetracarboxylic dianhydride, CBCDA, Ar_1), lead to poor electrical and ionic conductivity, resulting in limited capacities that are far below the theoretical values (Fig. S1 online) [14]. Given that prolonging the length of molecules with extended conjugated structure could improve the electrical conductivity, enhance the intermolecular interactions, and expand the packed structure [14,15], a series of dianhydride-based molecules, such as 1,2,3,4-cyclopentanetetracarboxylic dianhydride (CECDA, Ar_2), 1,2,3,4-pyromellitic dianhydride (PMDA, Ar_3), 1,4,5,8-naphthalene tetracarboxylic dianhydride (NTCDA, Ar_4), and 3,4,9,10-perylene tracarboxylic dianhydride (PTCDA, Ar_5), with the same active sites in terms of type, number, and position but increased conjugated structure were rationally selected to liberate their latent perfor-

mance, of which the charge storage mechanism was elucidated in Fig. S2 (online) in the case of the NTCDA. As shown in Fig. 1a, with the gradual extension of the conjugated structure from CBCDA to PTCDA, the capacity of PTCDA significantly increases (Fig. 1b and Fig. S3 online), but this could only be realized when the conjugated structure extends to a certain value (Ar_5). However, the increased inactive molecular weight during the extension of the conjugated structure leads to a decrease in theoretical capacity (273 mA h g^{-1} for CBCDA vs. 136 mA h g^{-1} for PTCDA; the corresponding calculation details are listed in Fig. S4 (online)), and this process cannot solve the challenge of poor cycling stability of OEMs (Fig. S5 online). Therefore, the original idea of extending the conjugated structure was transformed into constructing linear polymers using the aforementioned five dianhydride-based molecules as the basic building blocks to connect the linear linking point (i.e., 2,5-diaminocyclo hexa-2,5-diene-1,4-dione, DABQ, R_1) (Fig. 1c and Fig. S6 online). This structural evolution process can be regarded as the transition from point (dianhydride monomer) to line (linear polymer), and the corresponding reaction routes and material characterizations are shown in Fig. S6 (online). In addition to the goal of extending the structure, the construction of linear polymers could increase the molecular weight and enhance the interaction between adjacent polymer chains, contributing to the stability of the polymer structure and consequently preventing the dissolution of reaction intermediates during the discharge/charge process [16,17]. In addition, improved electrical conductivity could be realized by the polymerization-induced formation of continuous and large conjugated structures (Fig. 1d and Fig. S7 online) [18]. Notably, the steric hindrance between building blocks and linear linking points would cause chain rotation during polymerization, resulting in a specific spatial distribution of the active sites. Given that the storage of Zn^{2+} requires the coordination of adjacent active sites in the OEMs, the change in the steric hindrance during the evolution of the building blocks (i.e., Ar_1 to Ar_5) would certainly influence the Zn^{2+} ion storage properties of the obtained linear polymers because of the variable arrangement of their active sites [19]. As depicted in Fig. 1b and Fig. S8 (online), the reversible capacities of linear polymers show a trend of initial increase and subsequent decrease, indicating that simply enlarging the steric hindrance (i.e., Ar_1 to Ar_5) does not always increase the utilization of active sites, and high steric hindrance (Ar_5 here) would induce the mismatched arrangement of active sites. The linear polymer poly(1,4,5,8-naphthalenete tracarboxylic dianhydride/2,5-diaminocyclohexa-2,5-diene-1,4-di one) (PND, Ar_4 + R_1) with the optimized active site arrangement has a high reversible capacity and a long cycle life. These results indicate that the construction of linear polymers can not only increase the capacity but also solve the problem of poor cycling stability of OEMs, which cannot be realized by simply extending the conjugated structure. Despite its effectiveness, the entanglement of the linear polymer chains leads to the incomplete exposure of active sites, resulting in a loss of capacity.

To overcome the chain-induced entanglement, further structural evolution was designed to construct a polymer fabric with the interweavement of organic threads. As shown in Fig. 1e, the connection of the building block Ar_4 to the fabric linking point (i.e., 2,3,5,6-tetraaminocyclohexa-2,5-diene-1,4-dione, TABQ, R_2) successfully realizes the construction of a molecular fabric (PNT, Ar_4 + R_2; Fig. S9 online). That is, the structure evolves from point to plane. Notably, the fabric framework could avoid the entanglement of polymer chains and the disturbance of chains caused by ion coordination, increasing the exposure of active sites [20,21]. Moreover, the nearly parallel arrangement of organic threads makes them abundant space fields that could behave as noninterference "highways" for ion migration. Benefiting from these structural features, improved structural stability, electrical conductivity,
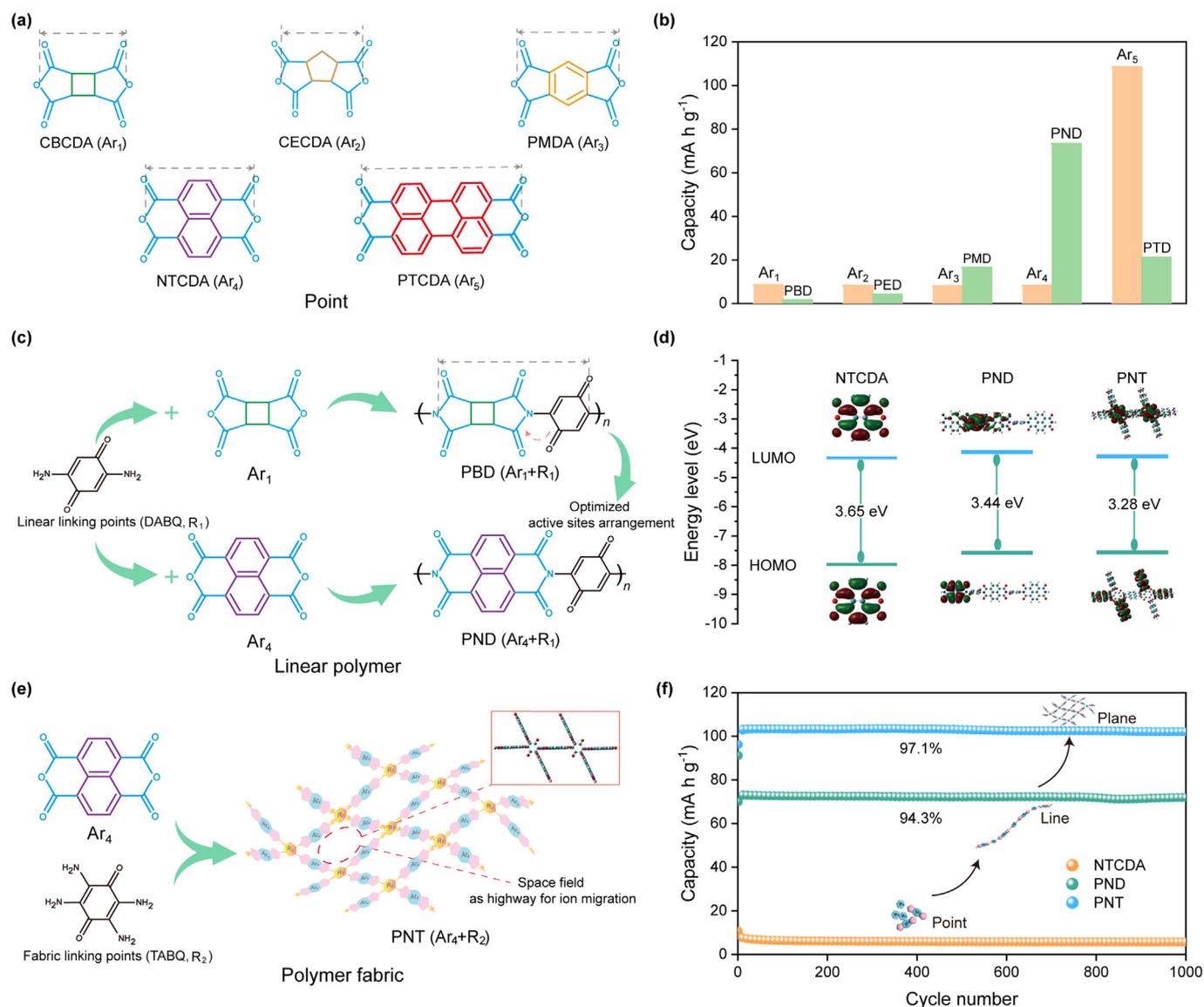
Fig. 1. (Color online) Design process of the polymer fabric and the electrochemical performance of the monomer-based and polymer-based cathodes in AZIBs. (a) Building blocks. (b) Capacity of the monomers and linear polymers at 50 C. (c) Design process of the linear polymers. (d) Highest occupied molecular orbital (HOMO) and lowest unoccupied molecular orbital (LUMO) energy levels and orbit distributions of NTCDA, PND, and PNT. (e) Design process and optimized configuration of PNT. (f) Electrochemical performance of NTCDA, PND, and PNT.

active site utilization, and ion diffusion kinetics could be obtained. As depicted in Fig. S10 (online), the *in-situ* variable temperature Fourier transform infrared spectroscopy (FTIR) analysis reveals the increase in thermodynamic stability as the structure evolves from point to line and plane (i.e., from NTCDA to PND and PNT), undoubtedly demonstrating an increasing trend in structural stability, which is advantageous in addressing the dissolution issue of OEMs during cycling. The thermodynamic stability of PNT can be further demonstrated by thermogravimetric analysis (TGA), where PNT shows an increased high-temperature resistance (Fig. S11 online). The increased structural expansion of PNT that enhanced the electrical conductivity can be demonstrated by its narrowest HOMO/LUMO energy levels and decreased charge transfer resistance (R_{ct}) of NTCDA, PND, and PNT (Fig. 1d and Fig. S7 online). Fig. 1f shows the clear improvement in both capacity and stability as the structures evolve from point to line and plane, and the transformation from line to plane increases the active site utilization from 37% to 79% (Fig. S12 online) and capacity retention from 94.3% to 97.1%. In addition, PNT exhibits high ion diffusion kinetics, which will be analyzed in the section on reaction kinetics.

Similarly, the advantages of our designed structural evolution process work well from PMDA (Ar_3) to poly(1,2,3,4-pyromellitic dianhydride/2,5-diaminocyclohexa-2,5-diene-1,4-dione) (PMD, $Ar_3 + R_1$) and poly(1,2,3,4-pyromellitic dianhydride/2,3,5,6-tetraa minocyclohexa-2,5-diene-1,4-dione) (PMT, $Ar_3 + R_2$) (Fig. S13 online). From the aforementioned results and analysis, we determine that our reasonable structural design realizes the simultaneous resolution of the issues of solubility, electrical and ionic conductivity, and active site arrangement encountered by OEMs in one material. The PNT polymer fabric with the most optimal structure for Zn^{2+} ion storage could also be a potential high-performance cathode for AZIBs. In the subsequent sections, the detailed electrochemical performance and ion storage mechanism of PNT were comprehensively investigated.

3.2. Electrochemical investigations of PNT

Fig. 2a depicts the cyclic voltammetry (CV) curves of PNT with a typical three-electrode system consisting of a Pt counter electrode and an Ag/AgCl reference electrode at 0.5 mV s^{-1}. Apart from the
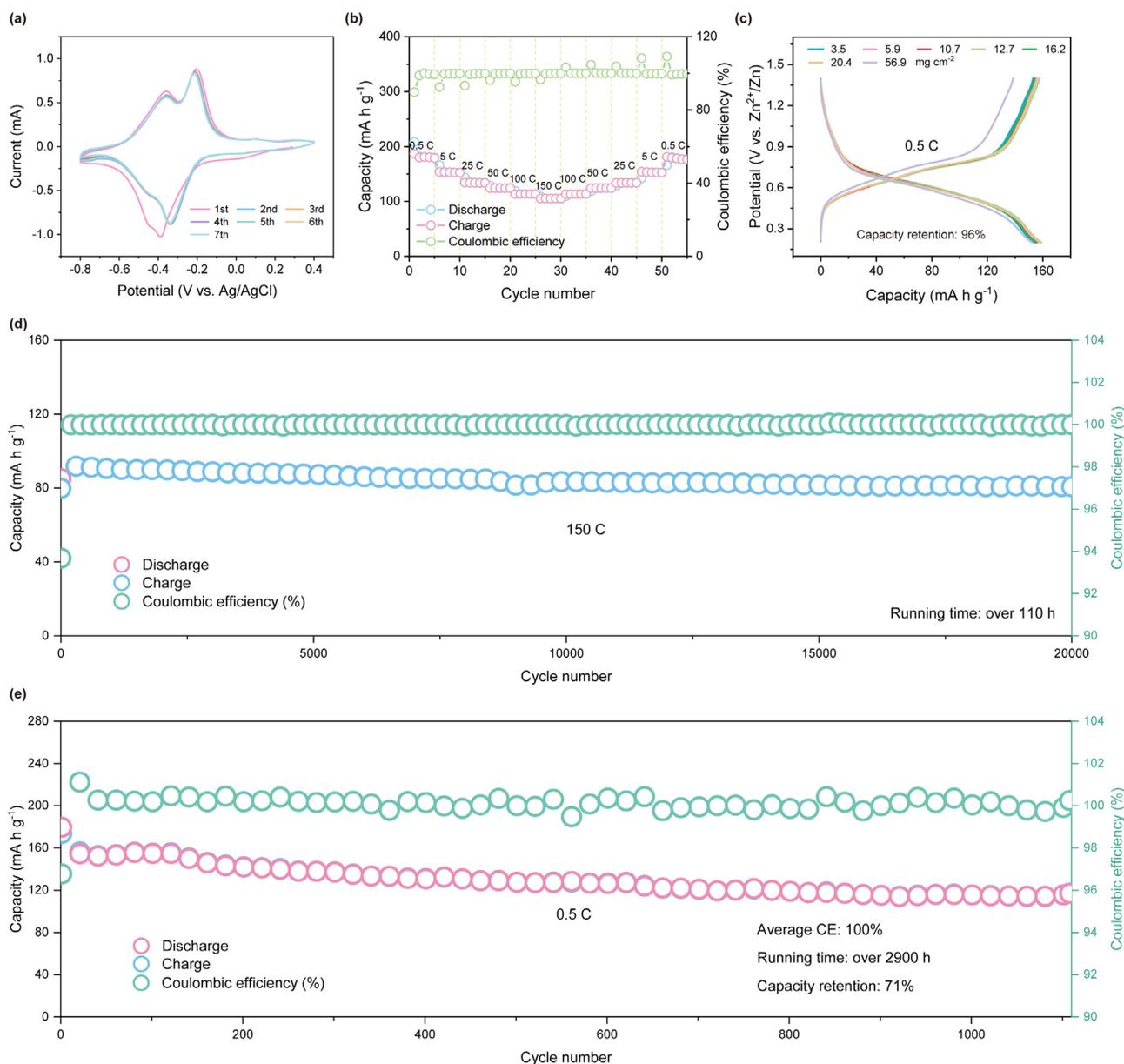
Fig. 2. (Color online) Electrochemical performance of the PNT//Zn batteries. (a) CV curves at 0.5 mV/s. (b) Rate performance at different current densities. (c) Discharge/charge curves at different mass loadings. Cycling performance at (d) 150 C and (e) 0.5 C.

initial activation process, the CV curves in the subsequent cycles exhibit minimal changes, signifying the high stability and reversibility of PNT in AZIBs [22]. In addition, two pairs of reduction and oxidation peaks corresponded to the conversion of C=O to C–O$^-$ and its associated reversible reaction could also be observed. Afterward, the rate capability of PNT was evaluated. As shown in Fig. 2b and Fig. S14 (online), PNT exhibits stable reversible capacities of 182, 166, 144, 129, 119, and 109 mA h g^{-1} at current densities of 0.5, 5, 25, 50, 100, and 150 C, respectively. Notably, when decreasing the current density from 150 C to 0.5 C step by step, the discharge capacity can recover to the initial value, revealing the superior rate capability and structural stability of PNT. Furthermore, the PNT cathode is surprisingly insensitive to the area mass loading (Fig. 2c). Even when the mass loading increased from 3.5 to 56.9 mg cm^{-2}, exceptionally high-capacity retention of 96% could still be maintained, which has never been realized in OEMs before (Table S1 online). (Note: The performance measurement was conducted in Swagelok®-type cells to avoid the

large pressure change in typical coin-type cells induced capacity decrease). This performance improvement can be ascribed to the existence of numerous noninterference ion migration channels in the fabric structure that enable Zn^{2+} to reach the vicinity of the active sites in the entire thick electrode. The PNT also delivers exceptional durability up to 20,000 cycles with a capacity fading rate of only 0.0004% per cycle at 150 C (average coulombic efficiency of 100%; Fig. 2d). The final failure of the battery may be caused by the side reactions from the zinc anode side that leads to its corrosion and passivation, limiting the continued operation of the battery. It should be mentioned that the structural advantages also endow the PNT with satisfactory cycling stability for over 2900 h with 71% capacity retention and 100% average coulombic efficiency at a low current density of 0.5 C, indicating that the rationally designed fabric configuration could well relieve the dissolution and structure damage issues of PNT (Fig. 2e). Collectively, the superior electrochemical performance of the PNT polymer fabric obtained here, such as the record-high-capacity

retention at high mass loadings and remarkable rate and cycling performance, proves the effectiveness of the fabric configuration in overcoming the performance liberation limitations of OEMs.

3.3. Origin of the outstanding reaction kinetics of PNT

To gain a deeper understanding of the exceptional rate capability and capacity retention of PNT, redox kinetic analysis based on the CV and galvanostatic intermittent titration technique (GITT) measurements were conducted. As the scan rate increases from 0.2 to 1.0 mV s^{-1}, both the shape and polarization of the CV curves experience no obvious change with the two well-maintained redox peaks (Fig. 3a). In addition, the relationship between the redox peak current i and the potential sweep rate v obeys the power law equation of $i = av^b$, where a and b are adjustable parameters [23]. A b value close to 0.5 indicates the diffusion-controlled electrochemical process, and a b value of 1.0 indicates the capacitance-controlled redox process [24]. Fig. S15 (online) depicts the logarithmic relationship between the peak current and the scan rate, and the b values of Peaks 1, 2, 3, and 4 are calculated to be 0.85, 0.94, 0.92, and 0.88, respectively. These high b values indicate that the capacitive behavior dominates the discharge/charge process of PNT, consequently resulting in rapid reaction kinetics [25]. Then, the capacity contribution percentage from the capacitive process at different scan rates was explored by dividing the specific capacity into the capacitance-controlled capacity ($k_1 v$) and diffusion-controlled capacity ($k_2 v^{1/2}$), written as $i = k_1 v + k_2 v^{1/2}$. Notably, the ratio of the capacitance-controlled capacity increases from 76.9% to 88.6% with the scan rate increasing from 0.2 to 1.0 mV s^{-1} (Fig. 3b and Fig. S16 online). Generally, a higher proportion of capacitance-controlled capacity could lead to a better rate capability [26].

To further support the rapid reaction kinetics of PNT, its Zn^{2+} diffusion coefficient (D) was estimated based on the GITT curves (Fig. 3c). As shown in Fig. 3d, the average D value of the discharge/charge process is $\sim 10^{-10}$ cm^2 s^{-1}, which is significantly higher than that of the linear polymer PND ($\sim 10^{-15}$ cm^2 s^{-1}; Fig. S17 online) and superior to most of the reported OEMs (Table S2 online). This large D value can be attributed to the numerous noninterference ion diffusion channels brought by the unique fabric configuration [27]. Moreover, the well-distributed covalent bonds in the polymer fabric could stabilize the structure during the discharge/charge process, ensuring that the initial storage/release of ions does not lead to structural damage that would hinder the subsequent ion diffusion [28,29]. The numerous high-speed ion migration pathways and the structural stability together contribute to PNT with rapid reaction kinetics and high-capacity retention even at high area mass loadings. Thus, PNT achieves outstanding cycling performance at 50 C with mass loadings of 3.4, 5.9, and 10.7 mg cm^{-2} (Fig. 3e) and exhibits high rate capability and reversibility at a mass loading of 12.7 mg cm^{-2} (Fig. S18 online), well demonstrating the superior Zn^{2+} ion storage properties of PNT.

3.4. Charge storage mechanism analysis of PNT

After confirming the excellent electrochemical performance of PNT, its energy storage mechanism was investigated. Fig. 4b shows the PNT electrodes monitored at different discharged and charged states (Fig. 4a) by *ex-situ* FTIR measurement. The blue regions at approximately 1706 and 1658 cm^{-1} represent the C=O vibrational mode in imide groups, and the orange region at 1573 cm^{-1} represents the C=O vibrational mode in quinone groups [30,31]. With the ongoing discharge process, the peaks corresponding to the C=O vibrational mode in both imide and quinone groups experience a steady decrease in intensity and eventually nearly disappear

at the end of the discharge process (Fig. 4b, from a to d), which can be ascribed to the transformation of C=O into C–O$^-$ anions. Upon charging to 1.4 V, the intensity of the C=O peaks shows a reverse tendency, indicating the reversible transformation from C–O$^-$ to C=O (Fig. 4b, from d to g). This reversible change in the C=O vibrational mode in both NTCDA building blocks and TABQ linking points powerfully supports the high electrochemical reversibility of PNT. Then, the *ex-situ* electron paramagnetic resonance (EPR) spectra were recorded to further validate the structural evolution of PNT. Fig. 4c shows the reversible shift of the *g*-value during the discharge/charge process. For the intermediate states (i.e., b, c, e, and f), the peak intensity is larger than that at the fully charged/discharged states (i.e., d and g) because of the higher concentration of the radical species (C–O$^-$) [32,33]. Aside from the FTIR and EPR measurements, the X-ray photoelectron spectroscopy (XPS) spectra of the PNT electrodes at different stages were also collected to check whether Zn^{2+} was involved in the electrochemical reactions (Fig. 4d and Fig. S19 online). From the O 1 s XPS spectra, we observe the reversible transformation between C=O and C–O$^-$ during a single cycle process (Fig. S19 online), which is consistent with the FTIR and EPR results. In addition, the transformation from C=O to C–O$^-$ accompanied by the increase in the peak intensity in the Zn 2p regions, and vice versa, proves the storage and release of Zn^{2+} in PNT during the discharge/charge process (Fig. 4d) [29].

Given the existence of Zn^{2+} and H$^+$ in the 1 mol L^{-1} ZnSO$_4$ aqueous electrolyte, the ion storage mechanism of PNT could involve the individual storage of Zn^{2+} or the co-storage of Zn^{2+} and H$^+$. Generally, OH$^-$ would continuously be generated through the consumption of H$^+$ during the discharge process in the ZnSO$_4$ electrolyte, and these OH$^-$ ions could readily react with ZnSO$_4$ to form Zn$_4$(OH)$_6$SO$_4\cdot$5H$_2$O. Such process is evidenced by the X-ray diffraction (XRD) patterns with the emergence of clear peaks from Zn$_4$(OH)$_6$SO$_4\cdot$5H$_2$O of the discharged PNT, and these peaks disappear in the subsequent recharge process (Fig. S20 online), confirming that H$^+$ is involved in the ion storage/release process of PNT [31]. In addition, the participation of H$^+$ in the ion storage/release process of PNT was further confirmed by performing a typical three-electrode CV measurement in the 1 mol L^{-1} ZnSO$_4$ and 5 $\times$ 10^{-4} mol L^{-1} H$_2$SO$_4$ electrolytes (Fig. S21 online). The concentration of the H$_2$SO$_4$ electrolyte selected here was according to the H$^+$ concentration in the ZnSO$_4$ electrolyte (pH $\approx$ 4), which could avoid the adverse effects of high H$^+$ concentration. In the CV curve of the H$_2$SO$_4$ electrolyte, two pairs of reduction and oxidation peaks corresponding to the keto–enol tautomerism of PNT can be observed. After shifting this CV curve based on the Nernst equation, the reduction and oxidation peaks partway overlap with the CV curve tested in the 1 mol L^{-1} ZnSO$_4$ electrolyte, which correspondingly demonstrates that the H$^+$ ions are indeed involved in the redox process of PNT even at such a low concentration [34].

Density functional theory (DFT) calculations were then employed to calculate the molecular electrostatic potential (MESP) distribution of PNT to judge the uptake of cations by its active centers from the thermodynamics point of view. From the MESP distribution of PNT, we observe that the areas around the carbonyl groups have negative ESP values (Fig. S22 online), indicating their roles as active sites for cation storage/release during the discharge/charge process. Furthermore, a total of 68 possible geometric configurations of PNT during the discharge process, recorded as PNT-H$_x$Zn$_y$ (where x and y are the numbers of stored H$^+$ and Zn^{2+}), were calculated as the reduction products at different discharge stages (n electrons, n = 1, 2, 3, 4; Fig. S23 online). The stability of PNT-H$_x$Zn$_y$ was considered by comparing the Gibbs free energies (G) to select the most stable geometric configuration. As shown in Fig. 4e and Fig. S23 (online), although the absolute values of the binding energy (E) and G of four H$^+$ with PNT are larger than the

J. Guo et al.
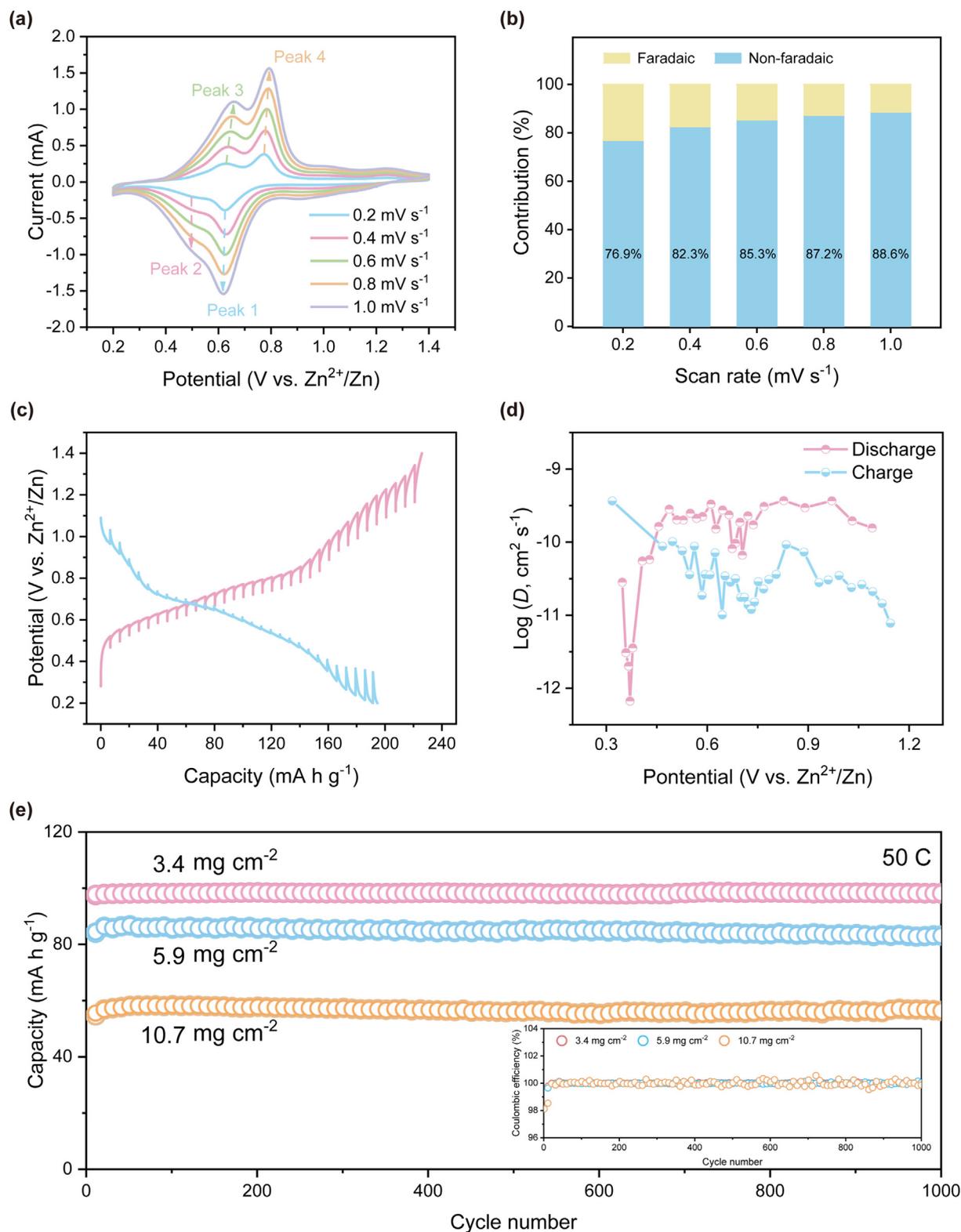
Fig. 3. (Color online) Analysis of the reaction kinetics of PNT. (a) CV curves and (b) contribution ratios of the capacitive charge storage at different scan rates. (c) Discharge/charge GITT curves. (d) Diffusion coefficient (D) toward Zn^{2+} estimated using the GITT method. (e) Cycling performance with different mass loadings at 50 C.

Zn^{2+}-containing configurations, such a PNT-H$_4$ structure is less likely to exist in the experimental condition where the concentration of Zn^{2+} is higher (approximately 10^4 times) than H$^+$ [19,35]. PNT-H$_2$Zn has a stronger binding energy than PNT-Zn$_2$ and has a more negative G value than PNT-Zn$_2$, indicating that PNT-H$_2$Zn is more thermodynamically favorable as the final discharge product. This ion storage process is also consistent with the experimental results. In summary, the previously presented analysis strongly supports the occurrence of the Zn^{2+} and H$^+$ co–(de)storage behavior in PNT during the discharge/charge process.
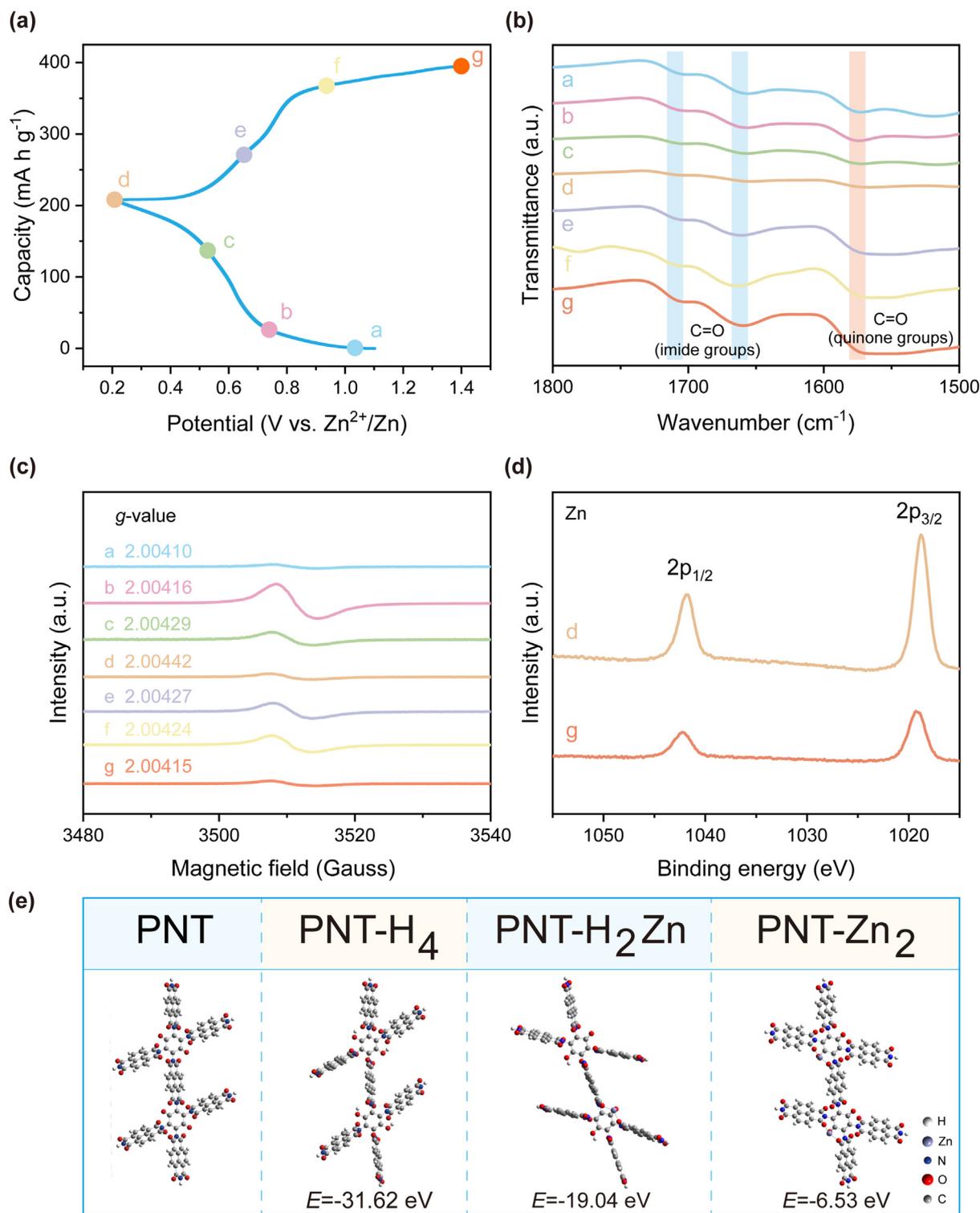
Fig. 4. (Color online) Energy storage mechanism of PNT. (a) Discharge/charge curves and the corresponding (b) FTIR, (c) EPR, and (d) XPS spectra of PNT at different electrochemical states. (e) Optimized geometries of PNT during the discharge process.

3.5. Suitability of PNT for Li⁺/Na⁺/K⁺ ion storage

Aside from its intrinsic stability and unique ion diffusion channels, PNT also has the potential to be a high-performance cathode material to store Li⁺/Na⁺/K⁺ in organic electrolyte systems. As illustrated in Fig. 5a, b, PNT exhibits a reversible capacity of 190 mA h g⁻¹ and superior rate performance when matched with the Li

anode. Large capacities of 190, 179, 167, 154, 144, 130, 107, and 87 mA h g⁻¹ could be delivered at the rates of 0.5, 2.5, 5, 15, 25, 50, 100, and 150 C, respectively. The discharge capacity can also recover to the original value when the current density is decreased from 150 C to 0.5 C, indicating that the superior rate capability achieved in AZIBs can be well inherited by the Li-ion batteries. Then, the reaction kinetics of PNT toward Li⁺ were investigated
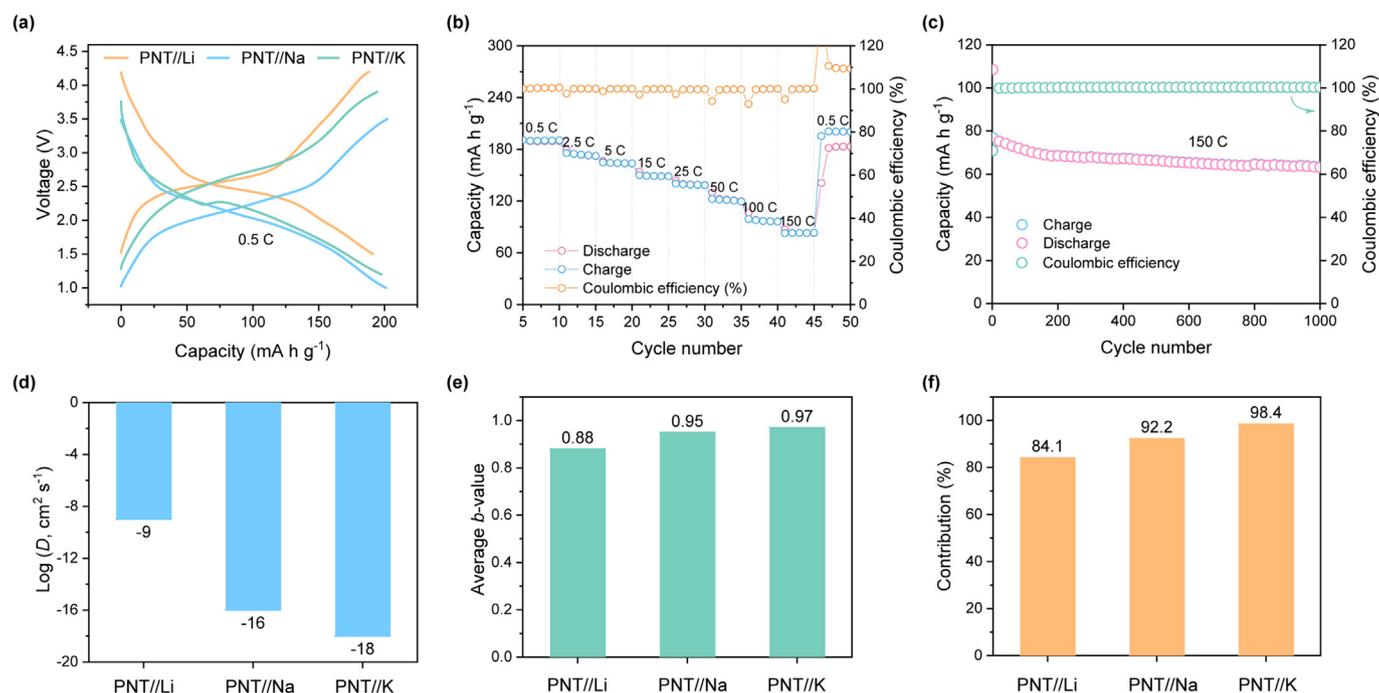
Fig. 5. (Color online) Electrochemical performance of the PNT//Li/Na/K-ion batteries. (a) Discharge/charge curves of the PNT//Li/Na/K-ion batteries. (b) Rate performance of the PNT//Li battery at different current densities. (c) Cycling performance of the PNT//Li battery at 150 C. (d) Diffusion coefficient (*D*) of PNT toward Li$^+$, Na$^+$, and K$^+$ estimated using the GITT method. (e) Average *b* values. (f) Contribution ratios of the capacitive charge storage of the PNT//Li/Na/K-ion batteries at 0.2 mV/s.

by conducting CV measurement at different scan rates (Fig. S24 online). According to the logarithmic relationship between the peak current and the scan rate ($i = av^b$; Fig. S25 online) [36], the *b* values of Peaks 1, 2, 3, and 4 are calculated to be 0.88, 0.93, 0.92, and 0.79, respectively, signifying that the capacitance-controlled behavior dominates the Li$^+$ storage/release process of PNT and thus resulting in rapid reaction kinetics in the Li-ion batteries as those in AZIBs. Meanwhile, the ratio of the capacity contributed by the capacitive process could reach 78.1%, 82.0%, 84.7%, 86.8%, and 88.8% at scan rates of 0.2, 0.4, 0.6, 0.8, and 1.0 mV s^{-1}, respectively, in the PNT//Li batteries (Fig. S26 online). PNT also exhibits stable cycling performance at both low and high current densities, i.e., over 100 h without capacity fading at 0.5 C and 76% capacity retention after 1000 cycles at 150 C (Fig. S27 online and Fig. 5c). In addition, just as expected, the average diffusion coefficient of PNT toward Li$^+$ (10^{-9} cm^2 s^{-1}; Fig. 5d and Figs. S28 and S29 online) is larger than that toward Zn^{2+} because of the smaller ionic radius of monovalent Li$^+$ (0.75 vs. 0.80 Å) [37], which supports the finding that the noninterference channels formed between the polymer chains can facilitate the diffusion of different ions. Similarly, when PNT is used as the cathode in Na/K-ion batteries, a high electrochemical performance could also be obtained (Fig. 5a and Figs. S30–S37 online). For comparison, the Na$^+$/K$^+$ diffusion coefficient of PNT was calculated, which follows the order of Li$^+$ > Na$^+$ > K$^+$ and is exactly the opposite order of their ionic radii (Fig. 5d). Moreover, the *b* value and the ratio of capacitance-controlled capacity increase with the enlargement of the ionic radius (Fig. 5e, f). As demonstrated previously, the structural advantages of PNT make it possess abundant noninterference channels for the efficient diffusion of ions with different sizes/valence states and high stability for guaranteeing applicability in both aqueous and organic electrolytes. These benefits together enable PNT to be a universal cathode in different energy storage systems.

4. Conclusion

In summary, an iterative design strategy of elaborately combining the building blocks from point to line (linear polymer) and plane (polymer fabric) has been proposed to overcome the long-lasting challenges that limit the full performance liberation of OEMs. The structural evolution from point to line not only effectively improves the structural stability and electrical conductivity but also adjusts the spatial distribution of active sites to facilitate the storage of Zn^{2+}. The evolution process from line to plane, in addition to the further enhancement of the aforementioned properties, could construct numerous noninterference channels for ion migration by the space fields from the nearly parallel arrangement of organic threads. As a result, the PNT polymer fabric with the most suitable structure realizes the simultaneous resolution of the issues of solubility, electrical and ionic conductivity, and active site arrangement encountered by OEMs. Consequently, the PNT polymer fabric exhibits outstanding Zn^{2+} ion storage properties, i.e., up to 20,000 cycles with a capacity fade of 0.0004% per cycle at 150 C and a capacity retention of 96% even with a high active mass loading of 56.9 mg cm^{-2}. Furthermore, the structural advantages make PNT a high-performance cathode for Li/Na/K-ion batteries with organic electrolytes. The results presented here provide insights into the full utilization of OEMs and guidelines for the design of advanced OEMs.

Conflict of interest

The authors declare that they have no conflict of interest.

Acknowledgments

Author contributions

Jun Guo performed experiments. Hongbo Chen performed DFT calculations and contributed to manuscript preparation. Dapeng Wang and Wanqiang Liu contributed to the analysis and discussion of the experimental results. Gang Huang and Xinbo Zhang directed research and contributed to manuscript preparation.

Appendix A. Supplementary material

Supplementary data to this article can be found online at https://doi.org/10.1016/j.scib.2024.08.010.

References

[1] Nguyen TP, Easley AD, Kang NA, et al. Polypeptide organic radical batteries. Nature 2021;593:61–6.
[2] Zhang XT, Li JX, Ao HS, et al. Appropriately hydrophilic/hydrophobic cathode enables high-performance aqueous zinc-ion batteries. Energy Storage Mater 2020;30:337–45.
[3] Lu Y, Zhang Q, Li L, et al. Design strategies toward enhancing the performance of organic electrode materials in metal-ion batteries. Chem 2018;4:2786–813.
[4] Chen Z, Cui HL, Hou Y, et al. Anion-chemistry-enabled positive valence conversion to achieve a record-high-voltage organic cathode for zinc batteries. Chem 2022;8:2204–16.
[5] Liang YL, Yao Y. Positioning organic electrode materials in the battery landscape. Joule 2018;2:1690–706.
[6] Wang CF, Li R, Zhu YC, et al. A pyrazine-pyridinamine covalent organic framework as a low potential anode for highly durable aqueous calcium-ion batteries. Adv Energy Mater 2024;14:2302495.
[7] Chu J, Liu Z, Yu J, et al. Boosting H$^+$ storage in aqueous zinc ion batteries via integrating redox-active sites into hydrogen-bonded organic frameworks with strong π-π stacking. Angew Chem Int Ed 2024;63:e202314411.
[8] Lee S, Hong J, Kang K. Redox-active organic compounds for future sustainable energy storage system. Adv Energy Mater 2020;10:2001445.
[9] Zhang H, Gao Y, Liu XH, et al. Organic cathode materials for sodium-ion batteries: from fundamental research to potential commercial application. Adv Funct Mater 2021;32:2107718.
[10] An SY, Schon TB, McAllister BT, et al. Design strategies for organic carbonyl materials for energy storage: Small molecules, oligomers, polymers and supramolecular structures. EcoMat 2020;2:e12055.
[11] Kumankuma-Sarpong J, Tang S, Guo W, et al. Naphthoquinone-based composite cathodes for aqueous rechargeable zinc-ion batteries. ACS Appl Mater Interfaces 2021;13:4084–92.
[12] Luo LW, Ma W, Dong P, et al. Synthetic control of electronic property and porosity in anthraquinone-based conjugated polymer cathodes for high-rate and long-cycle-life Na-organic batteries. ACS Nano 2022;16:14590–9.
[13] Qin KQ, Huang JH, Holguin K, et al. Recent advances in developing organic electrode materials for multivalent rechargeable batteries. Energy Environ Sci 2020;13:3950–92.
[14] Jin Z, Cheng Q, Bao ST, et al. Iterative synthesis of contorted macromolecular ladders for fast-charging and long-life lithium batteries. J Am Chem Soc 2022;144:13973–80.
[15] Qin KQ, Tan S, Mohammadiroudbari M, et al. Synergy of carbonyl and azo chemistries for wide-temperature-range rechargeable aluminum organic batteries. Nano Energy 2022;101:107554.
[16] Cang R, Song Y, Ye K, et al. Preparation of organic poly material as anode in aqueous aluminum-ion battery. J Electroanal Chem 2020;861:113967.
[17] Jing R, He J, Hu L, et al. A holomolecule conjugated and electron delocalized organic compound for superior proton-storage redox capability. Chem Eng J 2023;477:147169.
[18] Ma G, Ju Z, Xu X, et al. Enhancing organic cathodes of aqueous zinc-ion batteries via utilizing steric hindrance and electron cloud equalization. Chem Sci 2023;14:12589–97.
[19] Wang Y, Wang C, Ni Z, et al. Binding zinc ions by carboxyl groups from adjacent molecules toward long-life aqueous zinc-organic batteries. Adv Mater 2020;32:e2000338.
[20] Zheng S, Shi D, Yan D, et al. Orthoquinone-based covalent organic frameworks with ordered channel structures for ultrahigh performance aqueous zinc-organic batteries. Angew Chem Int Edit 2022;61:e202117511.
[21] Gao H, Neale AR, Zhu Q, et al. A pyrene-4,5,9,10-tetraone-based covalent organic framework delivers high specific capacity as a Li-ion positive electrode. J Am Chem Soc 2022;144:9434–42.
[22] Zhao Q, Huang WW, Luo ZQ, et al. High-capacity aqueous zinc batteries using sustainable quinone electrodes. Sci Adv 2018;4:eaao1761.
[23] Yang XR, Ni YX, Lu Y, et al. Designing quinone-based anodes with rapid kinetics for rechargeable proton batteries. Angew Chem Int Edit 2022;61:e202209642.
[24] Tie ZW, Zhang Y, Zhu JC, et al. An air-rechargeable Zn/organic battery with proton storage. J Am Chem Soc 2022;144:10301–8.
[25] Qin KQ, Holguin K, Huang JH, et al. A fast-charging and high-temperature all-organic rechargeable potassium battery. Adv Sci 2022;9:e2106116.
[26] Li S, Lin JD, Zhang YM, et al. Eight-electron redox cyclohexanehexone anode for high-rate high-capacity lithium storage. Adv Energy Mater 2022;12:2201347.
[27] Ye F, Liu Q, Dong HL, et al. Organic zinc-ion battery: Planar, π-conjugated quinone-based polymer endows ultrafast ion diffusion kinetics. Angew Chem Int Edit 2022;61:e202214244.
[28] Wang X, Xiao J, Tang W. Hydroquinone versus pyrocatechol pendants twisted conjugated polymer cathodes for high-performance and robust aqueous zinc-ion batteries. Adv Funct Mater 2021;32:2108225.
[29] Sun T, Li ZJ, Zhi YF, et al. Poly(2,5-dihydroxy-1,4-benzoquinonyl sulfide) as an efficient cathode for high-performance aqueous zinc-organic batteries. Adv Funct Mater 2021;31:2010049.
[30] Wang HG, Yuan S, Ma DL, et al. Tailored aromatic carbonyl derivative polyimides for high-power and long-cycle sodium-organic batteries. Adv Energy Mater 2014;4:1301651.
[31] Lin ZR, Shi HY, Lin L, et al. A high capacity small molecule quinone cathode for rechargeable aqueous zinc-organic batteries. Nat Commun 2021;12:4424.
[32] Tian Z, Kale VS, Wang Y, et al. High-capacity NH$_4^+$ charge storage in covalent organic frameworks. J Am Chem Soc 2021;143:19178–86.
[33] Bai YF, Wang Z, Qin N, et al. Two-step redox in polyimide: Witness by *in situ* electron paramagnetic resonance in lithium-ion batteries. Angew Chem Int Edit 2023;62:e202303162.
[34] Chen Y, Li JY, Zhu Q, et al. Two-dimensional organic supramolecule via hydrogen bonding and π-π stacking for ultrahigh capacity and long-life aqueous zinc-organic batteries. Angew Chem Int Edit 2022;61:e202116289.
[35] Gao YJ, Li GF, Wang F, et al. A high-performance aqueous rechargeable zinc battery based on organic cathode integrating quinone and pyrazine. Energy Storage Mater 2021;40:31–40.
[36] Chen T, Banda H, Yang L, et al. High-rate, high-capacity electrochemical energy storage in hydrogen-bonded fused aromatics. Joule 2023;7:986–1002.
[37] Agmon N. Isoelectronic theory for cationic radii. J Am Chem Soc 2017;139:15068–73.

Jun Guo is a Ph.D. candidate at School of Materials Science and Engineering, Changchun University of Science and Technology. His research interest focuses on the design and preparation of organic electrode materials and their application in electrochemical energy storage.

Hongbo Chen received his Ph.D. degree in Chemistry and Physics of Polymer from University of Chinese Academy of Sciences in 2018. In 2019, he joined Changchun Institute of Applied Chemistry, Chinese Academy of Sciences (CIAC, CAS) as an assistant researcher. His primary research focuses on using single-molecule fluorescence microscopy techniques and computational simulations to study the physics of polymer surfaces and interfaces.

Wanqiang Liu received his Ph.D. degree in Materials Science and Engineering from University of Jilin in 2008. In 2008, he joined CIAC, CAS as a lecturer, and in 2015 he was promoted to professor. His research focuses on design of electrode materials for rechargeable batteries.

Xinbo Zhang joined the CIAC, CAS as a professor in 2010. He received his Ph.D. degree in Inorganic Chemistry from CIAC, CAS in 2005. From 2005 to 2010, he worked as a JSPS and NEDO fellow at the National Institute of Advanced Industrial Science and Technology (Kansai Center), Japan. His interest mainly focuses on functional inorganic/organic materials for energy storage & conversion with fuel cells and batteries.

Gang Huang received his Ph.D. degree in Applied Chemistry from University of Chinese Academy of Sciences in 2016. Now he works at CIAC, CAS as a professor and his research focuses on the development and characterization of electrode materials for Li-metal and Zn-ion batteries.